



ELSEVIER

Surface Science 500 (2002) 84–104



www.elsevier.com/locate/susc

Electronic transport at semiconductor surfaces—from point-contact transistor to micro-four-point probes

Shuji Hasegawa^{a,b,*}, François Grey^c

^a Department of Physics, School of Sciences, University of Tokyo, 7-3-1 Hongo, Bunkyo-ku, Tokyo 113-0033, Japan

^b Core Research for Evolutional Science and Technology, The Japan Science and Technology Corporation, Kawaguchi Center Building, Hon-cho 4-1-8, Kawaguchi, Saitama 332-0012, Japan

^c MIC, Technical University of Denmark, Bldg. 345 East, DK-2800 Lyngby, Denmark

Received 27 July 2000; accepted for publication 24 April 2001

Abstract

The electrical properties of semiconductor surfaces have played a decisive role in one of the most important discoveries of the last century, transistors. In the 1940s, the concept of surface states—new electron energy levels characteristic of the surface atoms—was instrumental in the fabrication of the first point-contact transistors, and led to the successful fabrication of field-effect transistors. However, to this day, one property of semiconductor surface states remains poorly understood, both theoretically and experimentally. That is the conduction of electrons or holes directly through the surface states. Since these states are restricted to a region only a few atom layers thick at a crystal surface, any signal from them might be swamped by conduction through the underlying bulk semiconductor crystal, as well as greatly perturbed by steps and other defects at the surface. Yet recent results show that this type of conduction is measurable using new types of experimental probes, such as the multi-tip scanning tunnelling microscope and the micro-four-point probe. The resulting electronic transport properties are intriguing, and suggest that semiconductor surfaces should be considered in their own right as a new class of electronic nanomaterials because the surface states have their own characters different from the underlying bulk states. As microelectronic devices shrink even further, and surface-to-volume ratios increase, surfaces will play an increasingly important role. These new nanomaterials could be crucial in the design of electronic devices in the coming decades, and also could become a platform for studying the physics of a new family of low-dimensional electron systems on nanometre scales. © 2001 Elsevier Science B.V. All rights reserved.

Keywords: Electrical transport measurements; Scanning tunneling microscopy; Surface electrical transport (surface conductivity, surface recombination, etc.); Surface electronic phenomena (work function, surface potential, surface states, etc.); Silicon; Silver

1. Introduction

In many ways, the modern science of semiconductor surfaces was born along with the invention of the solid-state transistor in 1947 by William Shockley, John Bardeen and Walter Brattain. Prior to this date, work by Shockley and others to

* Corresponding author. Address: Department of Physics, School of Sciences, University of Tokyo, 7-3-1 Hongo, Bunkyo-ku, Tokyo 113-0033, Japan. Tel.: +81-3-5841-4167; fax: +81-3-5841-4167.

E-mail address: shuji@surface.phys.s.u-tokyo.ac.jp (S. Hasegawa).

make a field-effect transistor had failed. The driving idea behind the earlier attempts was simple; use a gate electrode, as shown in Fig. 1, to induce excess charges in a semiconductor, which travel through it as carriers of current flow, resulting in an increase in conductivity [1]. This kind of device already had been outlined in a prescient patent by Julius Lillienfeld in 1929. By changing the gate voltage, the conductance through the semiconductor could be varied. The gate was thus a tap that could control a flow of electrons—the prerequisite for amplification.

Alas, semiconductors resisted all attempts to fashion them into such a device. It took the ana-

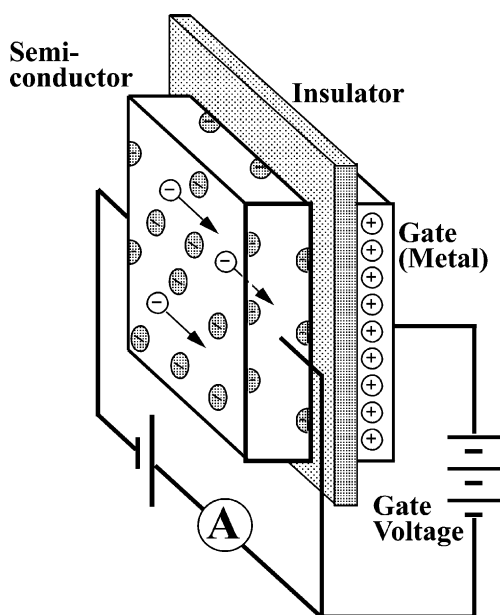


Fig. 1. Schematic of a field-effect transistor [1]. When a voltage is applied between a metal gate and a semiconductor, separated by a thin insulator, excess charges, negative ones on the semiconductor side, for example, are induced because of a capacitance of the structure. This should effectively vary the electrical conductance of the semiconductor, due to the change in number of carriers (electrons) flowing through it. Thus the gate voltage controls the current flow through the semiconductor, the basis of amplification. The field effect is diminished if there are surface states at the semiconductor–insulator interface, because they screen the electric field due to the gate by capturing the induced charges. Thus minimizing the amount of electronic states at the interface is a key requirement for field-effect transistor action.

lytical mind of Bardeen to realize what was going wrong. Bardeen postulated that there were charged electronic states at the semiconductor surface, which were screening out the electric field induced by the gate [2]. In other words, the induced charges are trapped in the surface states, becoming immobile. Thus the charges in the bulk of the semiconductor hardly felt the effect of the gate, and the current flow could be modified only minimally. This was a great insight, because not only did it explain a known phenomenon, but also it suggested ways to mitigate it. Together with Brattain, the experimental genius behind the first transistor, Bardeen began searching for ways to mitigate the screening effect. The result was the first point-contact type transistor, as shown in Fig. 2, in which two metal needles with a small spacing were brought into contact to a germanium crystal surface [3]. A current was injected into the crystal through the first needle (emitter), and electric potential distribution near the point contact was investigated with the second needle (collector) as a probe, as a function of the voltage applied to the germanium crystal via the base electrode.

Brattain and Bardeen discovered amplification during such measurements; a voltage signal fed through the emitter is transmitted to the collector as a larger voltage signal. The degree of amplification depends on the voltage of the base electrode. In one of the great ironies of technological history, what the researchers had made was not a field-effect transistor at all, but rather a precursor to modern bipolar transistors [4], where the surface states play a less important role, rather minority carriers injected into the bulk states are crucial for the transistor action. Nevertheless, when field-effect transistors were finally fabricated successfully some years later, it was due to Bardeen's insight. In particular, a key breakthrough was finding a surface where the number of surface states could be drastically reduced, greatly diminishing the shielding effect. This surface (or interface) was between silicon and silicon oxide. Interfaces involving the silicon(100) crystallographic surface showed the lowest density of the states, and for this reason, this crystallographic surface is still the most popular for modern electronic chip fabrication.

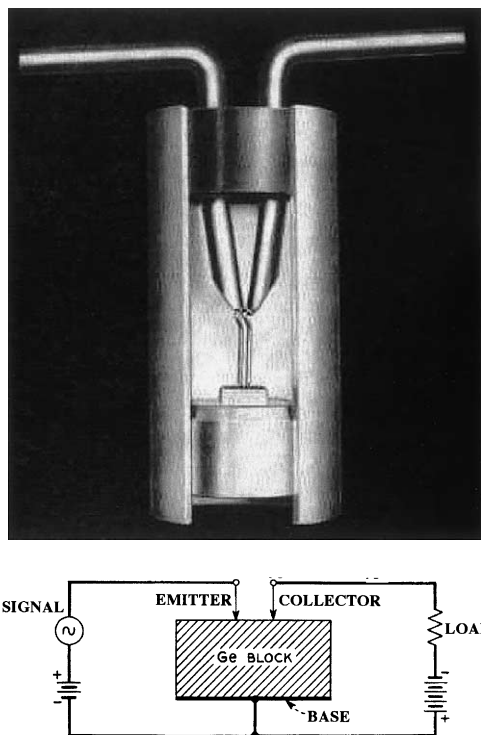


Fig. 2. A point-contact transistor of the type invented by Brattain and Bardeen [3]. The cutaway model shows the semiconductor at the center, below the two point contacts. Typical dimensions of the semiconductor were a couple of millimetres. The casing around the device protected the contacts from changes in ambient conditions that could affect the contacts. Below is a schematic diagram of the electrical circuit for the transistor action.

By the standards of modern surface science, the surface of the Germanium crystal that Brattain and Bardeen used in their pioneering experiments was dirty and ill-defined, since the experiments were carried out in air. Bardeen's idealized picture of surface states probably never applied to such surfaces. But today, under ultra-high vacuum (UHV) conditions in which the number of residual gas molecules is less than in the outer space, it is possible to tailor the crystallographic structure of semiconductor surfaces accurately, for example, by dosing the surface with small amounts (around a monolayer) of specific materials under precise control. As a result, a variety of *surface superstructures*—peculiar, but regular atomic arrangements of the topmost atomic layers on surfaces, a

kind of two-dimensional (2D) crystals—are created [5]. There is an intimate and profound relation between the crystallographic structure of a material and its electronic properties. This is well known for three-dimensional (3D) crystals (consider insulating diamond and conducting graphite, both of which are consisted of carbon atoms). It is also true of the 2D periodic structures at crystal surfaces.

What would Brattain and Bardeen have discovered with their two-point probe, had they had access to the well-defined surface states that can be produced today? Oddly enough, although their experiments are over 50 years old, there has been a long hiatus in surface science, during which comparatively little research was carried out on the electronic transport properties of surface states. In the same period, much has been learned about the atomic structure of surfaces, using techniques such as the diffraction of electrons and X-rays, and also about the surface-state electronic structure using primarily photoemission spectroscopy [6]. The scanning tunnelling microscope (STM), which can be compared to working with just one of Brattain and Bardeen's two probes [7], has helped to elucidate both atomic and electronic structure of surfaces. Indeed, STM has even detected transport through surface states on metals, albeit indirectly through the standing wave patterns that such conduction leads to [8,9]. But in the last few years, a new set of tools has been developed for more direct measurements of the transport, microscopic multi-probes, more similar to Brattain and Bardeen's original probes. These tools are revealing that semiconductor surface states have their own unique electronic transport properties. In a sense that Bardeen might have found amusing, history has come full circle.

In the next section, general descriptions of the interest in the electronic structures and electrical conduction at semiconductor surfaces are given. In Section 3, model systems on a Si(111) surface are shown to give a flavour of a huge variety of surface superstructures and surface states on a silicon crystal. Section 4 is devoted to results of surface-state transport obtained with recently developed probes. These are just an opening of the entrance to a rich field of study on the transport properties of surface states.

2. Surface-state bands and electrical conduction

2.1. What is a semiconductor surface state? And what is so special about it?

At the surface of a crystal, the atomic bonding geometry in the bulk is no longer necessarily the minimum free energy configuration. Atoms at the surface lack neighbours *above* them. For semiconductors such as silicon and germanium, the bonds are highly directional (covalent nature). So-called *dangling bonds*, unpaired bonds pointing in the direction of missing neighbours, are very reactive. These bonds naturally want to pair up with other unsaturated bonds on other surface atoms. The result can be a quite drastic change in the atomic arrangement in only one or two atomic layers on a crystal surface, leading to a lower free energy, but also a completely new periodic structure. This is a *surface reconstruction*, result of which is a *surface superstructure*. For example, the 7×7 superstructure of the (111) clean surface of a silicon crystal refers to a structure with a unit cell that is 49 times larger than that of the ideal surface, as described later in detail [10]. This is a resultant atomic arrangement of the minimum free energy at the clean surface, leads to only 19 dangling bonds, much fewer than on an unreconstructed surface. Furthermore, the same surface can go through a variety of complete structural rearrangements on absorption of only a fraction of a monolayer of foreign atoms to attain the lowest surface free energy [5]. These are *adsorbate-induced surface superstructures* in which atomic arrangements are in general quite different from those of the corresponding bulk alloys and compounds.

The periodic nature of a crystal leads to energy bands in which electrons occur: a valence band, which is practically full of electrons, and a conduction band, which is almost empty. Between them, a forbidden energy gap opens up (Fig. 3). The physics behind this is similar to diffraction of photons of X-rays in crystals; at some wavelengths and energies, a travelling wave is forbidden. In a map of wave energy against inverse wavelength (k -vector) of electrons (E - k space, or dispersion relations), the regions where travelling waves are allowed have the shape of energy bands (see Fig.

3(c)). When the periodic structure at the surface of a crystal is different from the bulk of the crystal, the allowed energy bands for electrons on the surface atomic layers may be different from those in the bulk. This is *surface-state bands*.

Sometimes an electron energy level in the allowed surface-state band is at the same time a level where bulk electrons are forbidden. For semiconductors, such surface-state bands become particularly important. The surface-state bands can alter the behaviour of the so-called *surface space-charge layer* just under the surface, by attracting excess negative or positive charges into the surface states, which then has to be compensated by an equal and opposite charges accumulated in the space-charge layer, typically about $1 \mu\text{m}$ thick. This charging of the surface effectively alters the positions of the bulk energy bands in the vicinity of the surface, an effect called *band bending* (see Fig. 3(a) and (b)). In this way surface states are responsible for the phenomena of charge carrier accumulation, depletion and inversion near a semiconductor surface. Without going into detail here, it is worth noting that such effects have led to 2D electron gases (2DEG) in such space-charge layers, where the quantum Hall effect, field-effect transistor action, and a rich variety of other electronic transport properties have been found [11].

In this article, however, the focus is on the conduction properties of the surface-state bands themselves, not of the space-charge layer. An obvious effect is that, for example, if a surface-state band crosses the Fermi level—the energy level above which the electron states are empty and below which they are full at very low temperatures—which lies in the bulk-band gap of the semiconductor (a metallic character), the surface-state band could be conducting. So the surface has completely different electronic transport properties from the bulk crystal. As we illustrate in the following sections, this is exactly what is seen in some cases.

2.2. Electrical conduction at semiconductor surfaces

The most common way to measure the electrical conductivity is to use a four-point probe, as shown in Fig. 4(a). A current is made flow through the

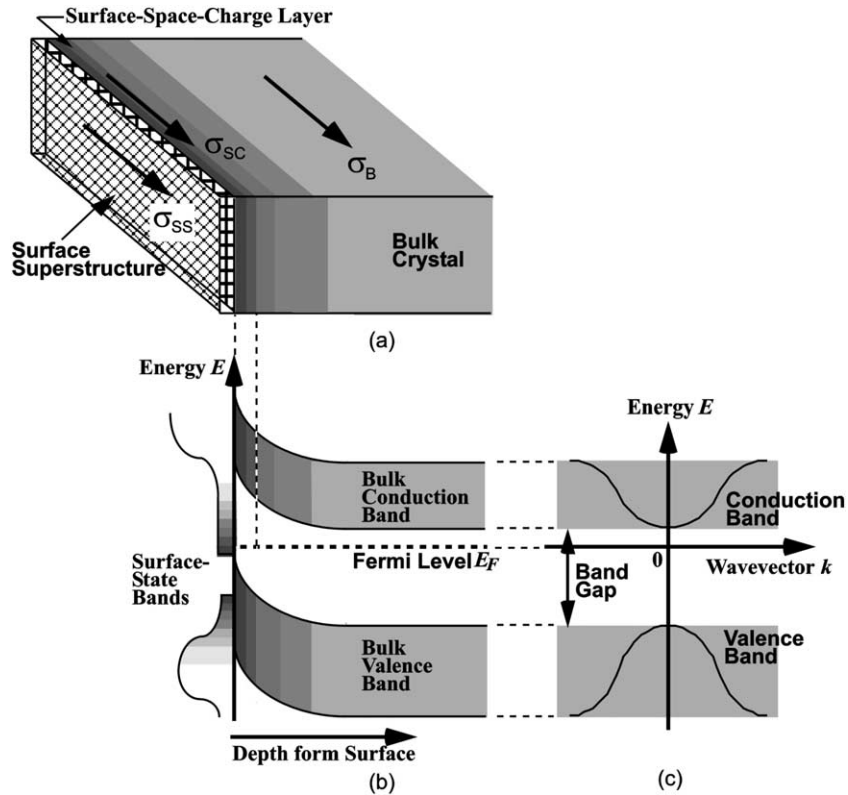


Fig. 3. Panel (a): Schematics of a semiconductor crystal, showing three channels for current flow; bulk states in the interior crystal (its conductivity is σ_B), surface-space-charge layer near the surface (σ_{SC}), and surface-state bands inherent in the surface superstructure at the topmost layers (σ_{SS}). Panel (b): An energy diagram near the surface, showing the bulk band structure, band bending beneath the surface, and surface-state bands. Panel (c): A band dispersion diagram, showing a relation between energy and wavevector of electrons in a crystal structure.

outer pair of probes, and a voltage drop is measured across the inner pair of probes, using a voltmeter with such large impedance that it draws hardly any current. As a result, the measured voltage drop V is predominantly that occurring across the semiconductor surface due to the current I flowing through the specimen. The four-point-probe resistance R of the sample is then obtained by $R = V/I$ (with a geometrical correction factor depending on the shape of specimen and probe spacing).

If we look more closely at the situation in Fig. 4(a), where the probes have macroscopic spacing (i.e. much larger than the thickness of the space-charge layer) in most cases, the current flows through three parallel channels [12]:

1. surface-state bands on the topmost atomic layers (when well-ordered surface superstructures are formed),
2. surface-space-charge layer due to band bending (in which conductivity can be considerably larger or smaller than in the bulk of the crystal in some cases),
3. unperturbed bulk bands inside the crystal (independent of the surface conditions and treatments).

The conductivity measured by a four-point probe method contains contributions from all of the three channels. In general it is very difficult to separate the contributions from each channel. For measurements made in air, without surface

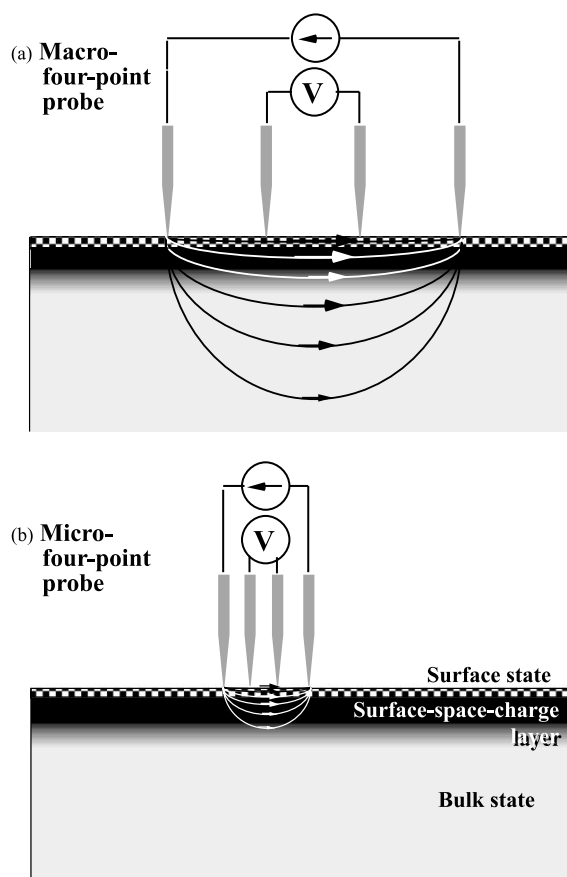


Fig. 4. Schematic diagram of a linear four-point probe measurement. A constant current source injects current through the left outermost probe, which is collected in the right outermost one. The potential difference measured across the inner probes, with a suitably high-impedance voltmeter, is then dependent only on the voltage drop across the specimen surface, eliminating contact resistance phenomena. Panel (a): Macroscopic probes in which the probe spacing is much larger than the thickness of the surface space-charge layer, and so most of the current passes through the bulk of the crystal. Panel (b): Microscopic probes, with schematic illustrations of current paths near a semiconductor surface, penetrating only a distance comparable to the spacing between the probes.

superstructures on the crystal, the measured resistance is normally interpreted as bulk resistance only. Possible contributions from the surface space-charge layer and surface-state bands are ignored. This is usually a good approximation, since on macroscopic scales, the surface-layer contributions are relatively small because a large

fraction of the current tends to flow through the interior of the crystal, far from the surface, as illustrated in Fig. 4(a). Despite this drawback, it has been possible in careful measurements with macroscopic probes to detect the effects of conductance through the surface space-charge layer, and in special cases also conductance directly through surface-state bands. As described in Section 4, these have been measured in UHV with crystals having well-ordered surface superstructures [13].

In the early days of surface science, a number of techniques were reported for measuring the surface conductivity of a semiconductor. In general, the data were interpreted in terms of conductivity in the surface space-charge layer, due to band bending, rather than the surface-state conductivity, because the latter was assumed (without much basis) to be negligible. Brattain and Bardeen [14] found that the band bending could be varied in a reproducible way by exposing the surface to different gaseous ambients (Brattain–Bardeen cycle). Since their experiments were not carried out with clean semiconductor surfaces in UHV environment, the gases adsorb randomly on the outer surface of the oxide film on the semiconductor in a form of ions, and electric fields due to these ions penetrate into the space-charge region across the oxide layer. The conductivity actually changed by varying the band bending due to the gas exposures. From the conductivity changes, reversibly, the amounts of band bending were deduced [15].

Changes in surface conductivity accompanied by conversions of surface superstructures in a well-controlled manner in UHV were first measured by Mönch and co-workers on clean Si and Ge crystals [16]. Their results showed a strong correlation between the structural conversion and change in surface conductivity, from which they could deduce a change in band bending under the surface. The band bending depends on the charge in the surface states, which redistributes due to the reconstruction of the surface atomic structure. In these pioneering experiments, the surface-state conductivity was not taken into consideration, because it was assumed to be negligibly small.

As described in Section 4, the surface-state electrical conduction has been confirmed first by a macroscopic four-point probe method through a

phenomena of carrier doping into a surface-state band [17], followed by other surfaces with conductive surface-state bands of metallic nature [13].

Another approach to detect and study the surface-state electronic transport is miniaturizing the four-point probes. By reducing the probe spacing to a distance similar to the space-charge layer thickness, as shown in Fig. 4(b), a larger fraction of the current flows near the surface because the current penetrates to an extent similar to the probe spacing. This results in a more surface-sensitive measurement than with the macroscopic four-point probes shown in Fig. 4(a) [18]. The actual current distribution in the crystal may not be as simple as illustrated in Fig. 4, because of a possible Schottky barrier between the surface states and the underlying bulk states [19] or a possible pn-junction between the surface-space-charge layer and the interior bulk. But, this simple picture appears to be at least qualitatively true, as demonstrated in recent measurements [20–23]. Two types of such microscopic four-point probes are introduced in Section 4.

The surface-state bands provide a new class of reduced-dimension electron systems, which may have the following new intrinsic features when compared with the other low-dimensional electron systems. Three forces described below drive the study of the transport properties of surface states.

(1) *Variety*: More than 300 kinds of surface superstructures are found on silicon crystals with foreign adsorbates of around monolayer coverages [5]. Their surface-state bands are known to show a rich variety of characters, some of which are introduced in Section 3. We can play with them to study almost all kinds of low-dimensional phenomena just on silicon surfaces. Furthermore, of course, more huge variety of surface states is also known on surfaces of other materials.

(2) *Scales*: As described in Section 3, some surface-state bands have a nearly 2D free-electron character, which is quite similar to the conventional 2DEG systems formed at the space-charge layers (Fig. 5). One of the main differences between them, however, is *thickness*. The surface-state systems are much thinner, around a monatomic thick, compared with a thickness of around 10 nm for the conventional 2DEG. This results in much

larger energy spacing between the quantized energy levels in the confinement potential wells normal to the surface. Therefore, we have to consider only the lowest energy level for the surface states even at room temperature, while the higher-energy levels are frequently involved in the phenomena at the conventional 2DEG systems even at low temperatures. Some other surface-state bands consist of 1D atomic chains only a few atoms wide, exhibiting some 1D nature. These may be the thinnest quantum wire known so far. Due to such small dimensions, we can tailor the surface states in a way that quantum effects suitable for nanometre-scale devices can be expected even for metals having short Fermi wavelengths.

(3) *Controllability*: The structures on surfaces can be precisely controlled and fabricated using *self-organization phenomena*—atoms spontaneously rearrange themselves to make regular surface superstructures, or using *atom/molecule manipulation* techniques—atoms are made arrange one by one with *atom tweezers* [24]. Surface-state transport may be controlled in a novel way when combined with such fabrication techniques of atomic-scale structures.

3. Silicon(1 1 1): a case study

To get a more quantitative picture of surface states of silicon crystals, one of the most popular materials in surface science, consider surface-state bands using the schematic illustration given in Fig. 6. When a Si atom makes a bond with a neighbouring atom, the energy level splits into bonding and anti-bonding states. The valence electrons are accommodated in the bonding state, so that the anti-bonding state is empty. Since in a crystal many atoms make bonds to each other to arrange themselves periodically, these energy levels are broadened to make bands, valence band and conduction band, respectively. These are electronic states in a bulk crystal (see also Fig. 3).

But on the surface, there are the dangling bonds, which have an energy level located between the bonding and anti-bonding states, or, within an energy gap of the bulk band structure. Actually, the dangling-bond state on a clean Si(1 1 1) surface

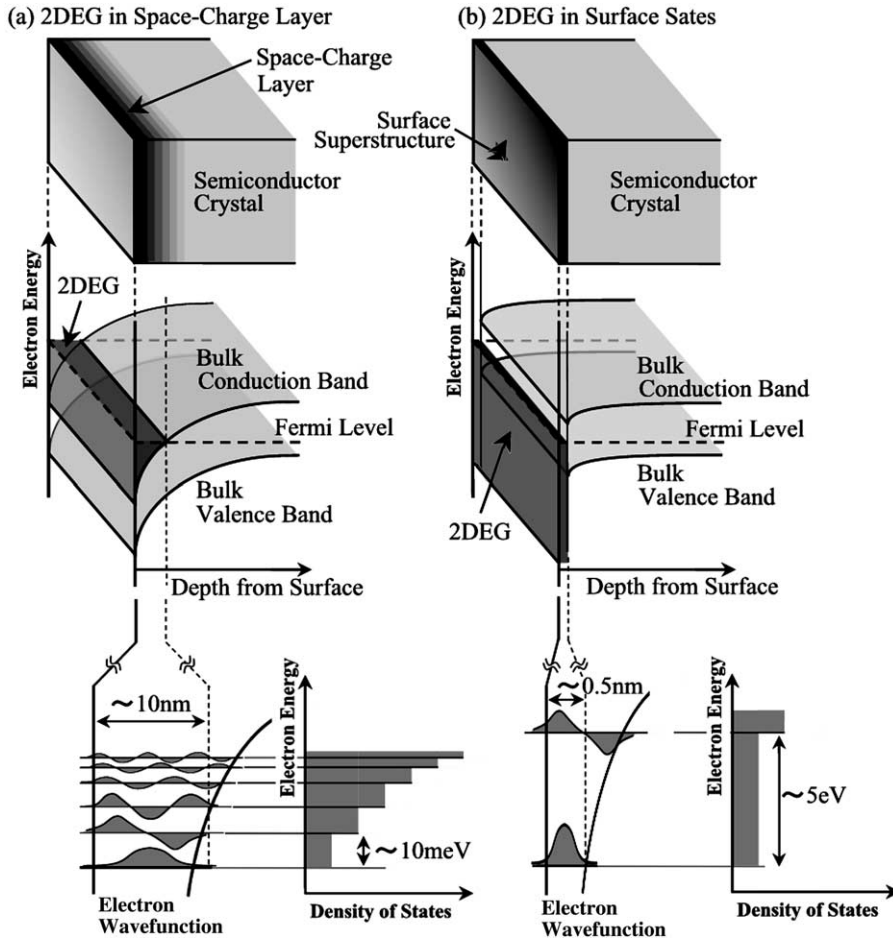


Fig. 5. Comparison of 2DEG systems between (a) at a surface space-charge layer and (b) at surface states. Upper panels: real-space illustrations showing where the 2DEGs are formed. Middle panels: energy band diagrams showing the electronic states of the 2DEGs. The former 2DEG (a) is formed in bulk state bands extending over 10 nm into the crystal, while the latter 2DEG (b), of which thickness is around 0.5 nm, is formed at the topmost few atomic layers on the crystal surface. Lower panels: potential wells and wavefunctions of the 2DEGs, and also their density of states. The spacing of energy levels is much larger in (b) than in (a) due to the much narrower well width.

is known to lie around the middle of the band gap [25,26]. But when foreign atoms bond with the topmost Si atoms, the dangling-bond state is again split into bonding and anti-bonding states. When, furthermore, the adsorbates induce a surface superstructure to generate overlaps between atomic orbitals of neighbouring sites, the bonding and anti-bonding states are broadened into bands. These are *surface-state bands*, inherent in the surface superstructure, which have their own character, independent of the bulk electronic states. To

give a hint of the great variety of surface-state band structures that can arise on silicon, we give three examples on a Si(111) crystal surface.

3.1. $\text{Si}(111)-\sqrt{3} \times \sqrt{3}\text{-Ag}$: a two-dimensional metal

The $\text{Si}(111)-\sqrt{3} \times \sqrt{3}\text{-Ag}$ surface superstructure is formed by depositing one monolayer (ML) of Ag atoms on a Si(111) surface at temperatures higher than 250 °C. One ML means an atom

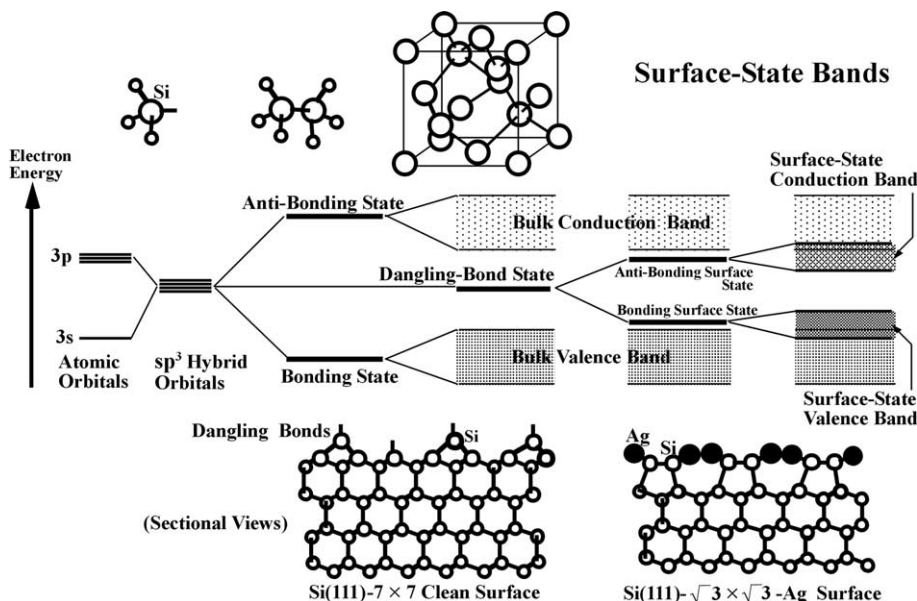


Fig. 6. A schematic illustration of energy diagram of atoms, molecules, and also in bulk and at surface of a silicon crystal. The valence electrons of an isolated Si atom are in 3p and 3s atomic orbitals. These orbitals are 'hybridized' into sp^3 orbitals when the atoms arrange in tetrahedral structures like in a diamond-lattice crystal and in SiH_4 molecules. When the atoms make bonds with the neighbouring atoms, the energy level of the orbitals splits into anti-bonding and bonding states. Furthermore, in the crystal the atomic orbitals overlap with each other between the neighbouring sites, the energy levels broaden into bands, conduction band and valence band, between which an energy gap opens. This is an electronic state in the bulk crystal of Si. The Si atoms on the topmost surface layer of the crystal, however, have dangling bonds, of which energy level is similar to the unpaired sp^3 hybrid orbitals, locating within the band gap. The dangling-bond state split into anti-bonding and bonding states when foreign atoms bond to the topmost Si atoms. These states are created only in the surface layer, surface electronic states. When the adsorbate adsorption induces a surface superstructure, the surface states become bands due to the overlap of surface states among the periodic atomic sites on the surface. These are surface-state bands. They have characters different from the bands in the bulk crystal because the atoms in the surface superstructure arrange in a way completely different from in the bulk crystal.

density equal to that of the topmost layer of Si(111) face, 7.8×10^{14} atoms/cm². The atomic arrangement of this surface is known to be a so-called honeycomb-chained triangle (HCT) structure as shown in Fig. 7(a) [27–29], in which each Ag atom makes ionic covalent bond with a substrate Si atom, leaving no dangling bonds, resulting in an exceptionally stable surface.

This surface has a characteristic surface-state band that is revealed by a technique called angle-resolved photoemission spectroscopy (ARPES) [30,31]. The surface-state band is parabolic and crosses the Fermi level (E_F), as indicated by S_1 band in Fig. 7(b). A parabolic band is characteristic of a 2D free-electron-like state, in other words, a state in which the electrons behave like free travelling waves along the surface. Furthermore,

this band is partially filled with electrons, a requisite of a metal, and confined only in the topmost layer of Ag and Si atoms. Therefore we can call this surface a 2D metal.

Such a 2D free-electron state can be visualized in low-temperature STM images in the form of so-called *electron standing waves* (more technically *energy-resolved Friedel oscillations* [32]). Such standing waves were first observed on metal surfaces independently by Eigler's group [8] and Avouris's group [9], and extended by several others [33–36]. They are essentially the consequence of electron travelling waves bouncing off steps and other defect structures, leading to a self-interference pattern that changes the probability for electrons tunnelling from the tip into the sample surface. Although not a direct measurement of

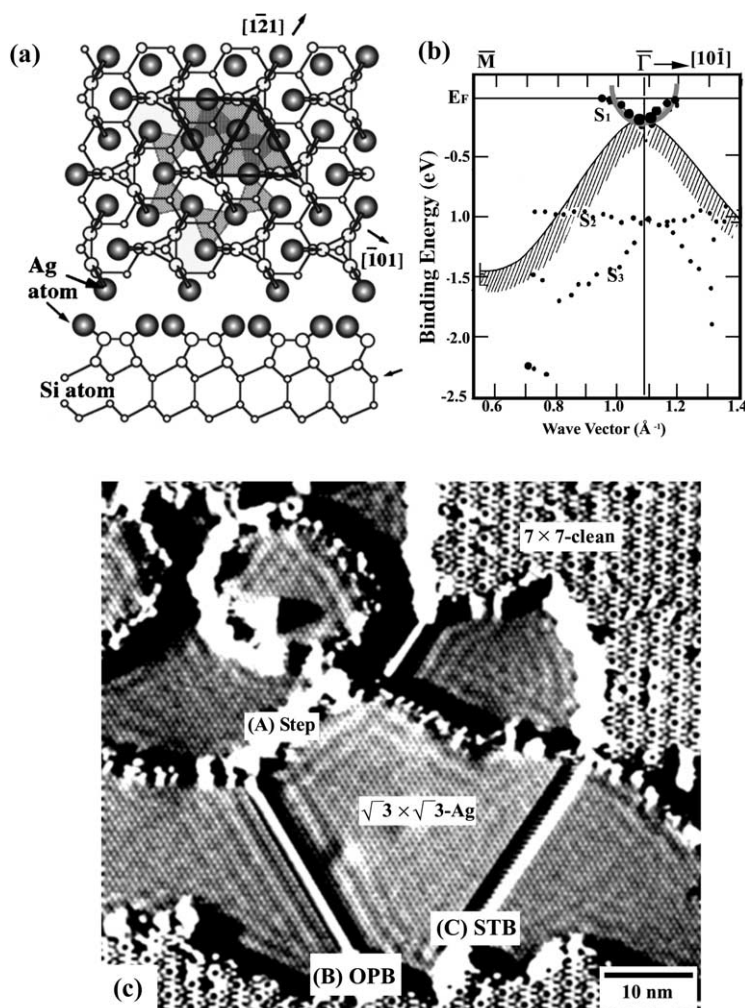


Fig. 7. Panel (a): Schematic illustrations of atomic arrangements (upper panel: plan view, lower panel: sectional view) of the Si(111)- $\sqrt{3} \times \sqrt{3}$ -Ag surface superstructure (a HCT model [27]). Panel (b): Its band dispersion diagram showing surface-state bands, constructed by angle-resolved photoemission spectroscopy measurements [57]. The shallowest state S_1 has a parabolic shape crossing the Fermi level E_F , indicating a nearly free-electron character. The curve with hatching shows a projected region of the bulk bands of a silicon crystal. $\bar{\Gamma}$ and \bar{M} indicate symmetric points in the $\sqrt{3} \times \sqrt{3}$ surface Brillouin zone. Panel (c): An empty-state STM image of this surface (partially the 7×7 domains remain) taken at 6 K [32]. ‘OPB’ is an out-of phase domain boundary at which a mismatch in the $\sqrt{3} \times \sqrt{3}$ -periodicity occurs between the adjacent domains. ‘STB’ is a ‘surface twin boundary’ at which domains in twin relation in structure meet [31]. Ripples are observed near step edges (A) and OPBs (B), while no observable ripples at STB (C). This means that the steps and OPBs act as potential barriers for surface-state electrons to ‘reflect’ the electron waves, resulting in an interference between the incident and reflected waves to form the standing wave patterns.

surface transport, they provide indirect proof of the free-electron nature of the surface-state electrons.

Fig. 7(c) shows an STM image of the $\sqrt{3} \times \sqrt{3}$ -Ag surface taken at 6K (though the 7×7 clean domains partially remain, because of a Ag cover-

age smaller than 1 ML). In the $\sqrt{3} \times \sqrt{3}$ -Ag domains, fine periodic corrugations are seen, corresponding to the periodicity of this superstructure. Additionally, one can see standing wave patterns superimposed near step edges (A) and domain boundaries (B). In a small domain on the

upper right, surrounded by steps and domain boundaries, a complicated concentric interference pattern is observed, while near the straight domain boundaries, the interference patterns are parallel to the boundaries.

These interference patterns raise some important questions for surface-state electronic transport: For example, what is the transmission coefficient of electron wavefunction at such boundaries? This governs an important parameter, the mobility of surface-state carriers. Certainly from Fig. 7(c), one can deduce that the carrier mobility must be lowered by carrier scattering by the step edges and domain boundaries. But, by how much? The mobility of the surface-state electrons on the $\sqrt{3} \times \sqrt{3}$ -Ag surface has been measured to be lower than that in the bulk crystal by two orders of magnitude [17]. But at present, there is no consensus on what role the carrier scattering from step edges plays in this difference.

3.2. The Si(111) 7×7 surface: a poor metal or Mott insulator?

For the 7×7 clean surface without any foreign atoms adsorbed (Fig. 8(a)) [10], the electrons which contribute to the surface state are those on the remaining dangling-bonds on the surface atoms, which are also those that contribute to the STM images. Since these Si atoms are not the nearest neighbours (filled circles in Fig. 8(a)), there is very little overlap between their electron wavefunction. The degree of overlap controls how the curvature of the surface-state band in E - k space. On the $\sqrt{3} \times \sqrt{3}$ -Ag surface the overlap is large, hence the parabolic shape of the surface-state band S_1 (Fig. 7(b)). On the 7×7 surface the small overlap leads to an almost flat surface state (nearly no variation of energy with k -vector), as shown by S_1 band in Fig. 8(b).

As a result of this difference, electrons on the 7×7 surface behave much more as isolated states than as travelling waves. This is the reason why there are no observable standing waves on the 7×7 domains in Fig. 7(c), even though the surface state is very close to the Fermi level, suggesting a metallic behaviour. The actual position of S_1 band in Fig. 8(b) is disputed; if it crosses the Fermi level,

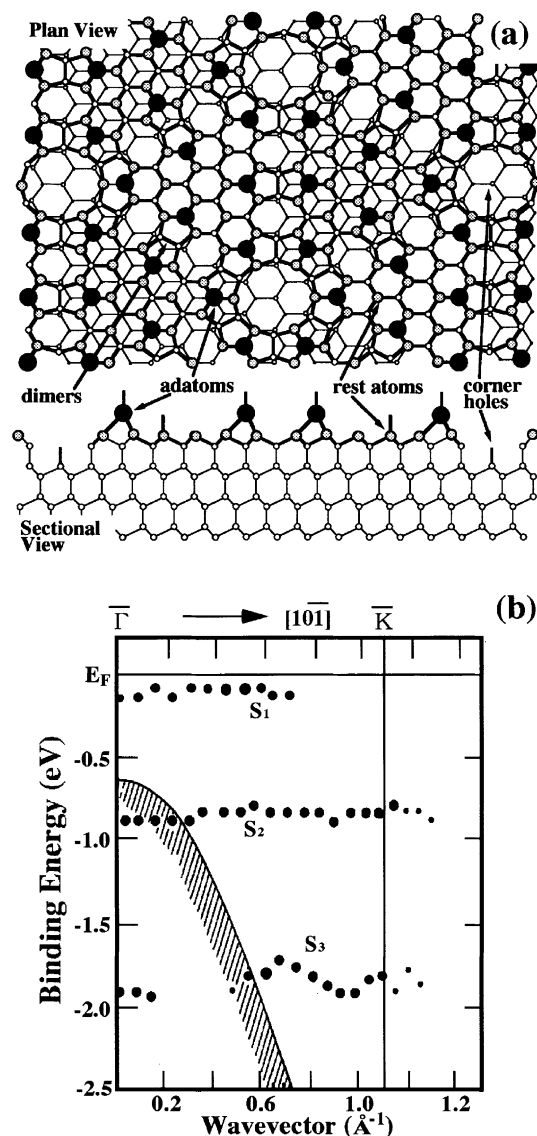


Fig. 8. Si(111)- 7×7 clean surface. Panel (a): Schematics of the atomic arrangement. Every circles indicate Si atoms, but have different names. Filled circles: adatoms. Shaded circles: rest atoms. The 7×7 unit cell is a lozenge having the corner at 'corner holes'. Panel (b): Its band dispersion diagram, constructed by angle-resolved photoemission spectroscopy [13]. The shallowest state S_1 shows an almost flat band, indicating its localized character. This is the dangling-bond surface state of the topmost Si atoms (filled circles in (a)). The curve with hatching shows a projected region of the bulk bands of a silicon crystal. $\bar{\Gamma}$ and \bar{K} indicate symmetric points in the 1×1 surface Brillouin zone.

then strictly the surface is metallic [37]. Otherwise an energy gap opens up around the Fermi level, or Mott insulator [38]. Temperature dependent measurements of electrical conductivity through this state, as yet unavailable, could help to distinguish between these two possibilities. Because of this localized nature, the surface-state conductivity is measured to be four orders of magnitude lower than that of the $\sqrt{3} \times \sqrt{3}$ -Ag surface, as discussed further on in this article [19].

3.3. $\text{Si}(111)\text{-}4 \times 1\text{-In}$: a one-dimensional metal

The final example, $\text{Si}(111)\text{-}4 \times 1\text{-In}$ surface superstructure is formed by depositing 1 ML of In atoms on a $\text{Si}(111)$ surface at around 300 °C. Its atomic arrangement is still a matter of debate [39], but one model is shown in Fig. 9(a) [40,41]. According to this model, indium atoms arrange in four lines, between which a zigzag Si chain runs. As one can imagine from this atomic arrangement, its surface electronic state is highly anisotropic. From photoemission spectroscopies [42,43], it is metallic along the In chains, while insulating in the perpendicular direction. In other words, the electrons are mobile along the In chains, while they can hop only with considerable energy to neighbouring chains. This is the recipe for a 1D metal.

The properties of a 1D metal have been appreciated since the early days of quantum mechanics, because solving Schrödinger equation is much easier in 1D than in 2D or 3D. Easier it may be, a 1D metal is inherently unstable. It spontaneously develops some sort of periodic lattice distortion known as a Peierls instability [44]. A charge-density wave (CDW)—a spatially periodic modulation in electron density—accompanies with the distortion to lower the electronic energy.

Fig. 9(b) is an STM image of the $4 \times 1\text{-In}$ surface taken at 70 K, showing stripes corresponding to the In chains in four lines given in Fig. 9(a). Along each stripe, one can clearly see the modulations with the double periodicity [45]. The ripples are not so clear on some stripes, due to fluctuations of the structure. A range of other surface science techniques has confirmed that this is a Peierls state, and the ripples are 1D CDW accompanied with a lattice distortion [45,46] (al-

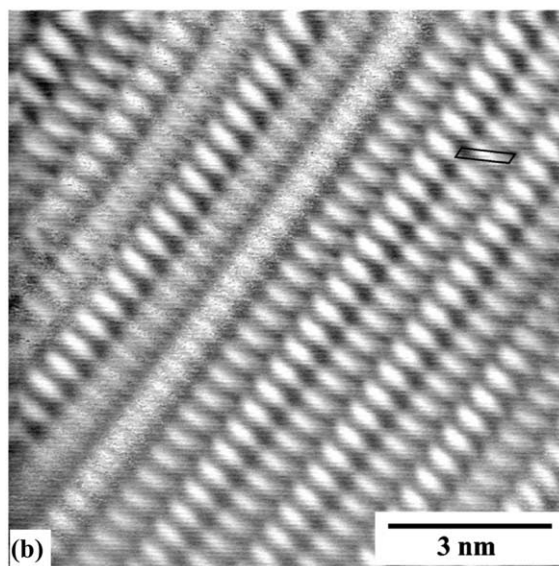
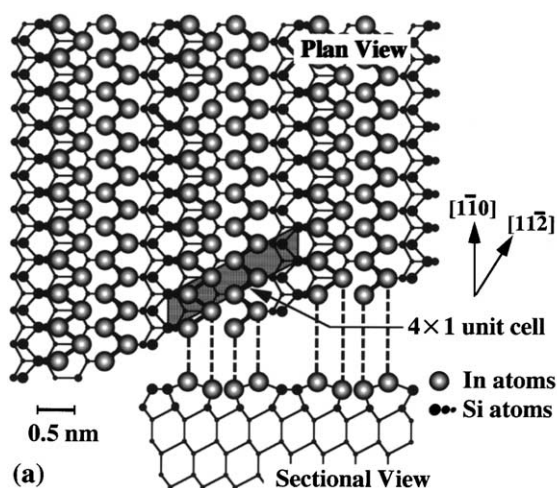


Fig. 9. Panel (a): A model of atomic arrangement of the $\text{Si}(111)\text{-}4 \times 1\text{-In}$ surface [40]. Shaded big circles are indium atoms, and the others are Si atoms. Panel (b): Its empty-state STM image at 70 K [45]. A 4×1 unit cell is indicated by a parallelogram. Each stripe corresponds to the four lines of In atoms shown in (a). Modulations of the double periodicity are seen along the stripes, which is due to charge-density waves.

though the latest study casts a doubt against this picture [47]). The surface-state transport must be influenced by this Peierls transition. Although such transitions are known to occur at quasi-1D bulk materials [48,49], the $4 \times 1\text{-In}$ surface was the first surface state to show this phenomenon.

4. Measuring surface-state transport directly

So far, only indirect measurements of transport of electrons through surface states, in particular the signature of metallic surface states observed by various spectroscopic methods including STM, have been described. But the double probes used by Brattain and Bardeen are not common tools in surface science. In this section, experimental techniques are described which are natural descendants of the point contact transistor, and which are paving the way for a deeper understanding of transport in surface states.

4.1. 'One-point' probes

As described in Section 2, four-point probes provide the most accurate and direct way of measuring surface transport properties. Nevertheless, much has been learned about the transport with a 'one-point' probe—the STM tip. So some of the outstanding results obtained so far with this technique are considered in this subsection.

Hasegawa(Y), Lyo, and Avouris [50] suggested that the electrical conduction through the dangling-bond surface state on the Si(111)- 7×7 is detected as an excess leakage current at a nanometre-scale point contact between the STM tip and the silicon surface. As the radius r of the contact area is reduced to nanometre scale, the current flowing through the metal/semiconductor interface at the contact is reduced in proportion to r^2 , while the leakage current through the periphery of the contact area is proportional to r . Therefore the leakage dominates at nanometre scale contacts. The current flows along the surface under such a condition, not directly into the crystal, which is illustrated in the inset of Fig. 10. This is a reason one expects to obtain the surface-state conductivity by this method.

Fig. 10 shows the conductance between the tip and specimen, measured as a function of tip displacement towards the clean Si(111)- 7×7 surface, together with the data for a clean Si(100) and Au surfaces for comparison [50]. In a tunnelling regime, where the tip-sample distance is larger (0–0.5 nm range in the horizontal axis), the conductance increases exponentially with decrease of

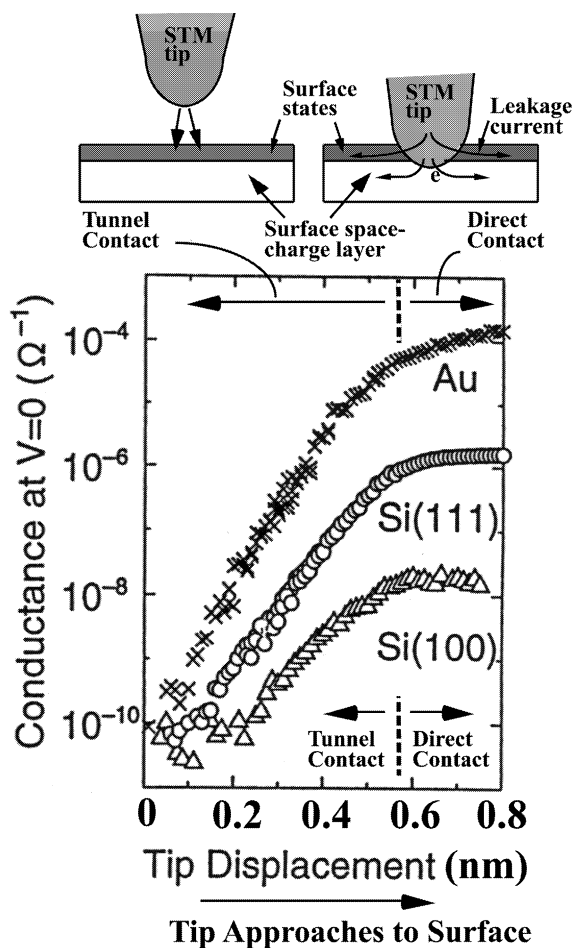


Fig. 10. Conductance between a STM tip and specimen surfaces, as a function of tip displacement toward the Si(111)- 7×7 surface, Si(100)- 2×1 surface, and polycrystalline Au surface, respectively [50]. The upper panels illustrate current flows at tunnel regime (left) and at direct contact (right), respectively.

the tip-sample distance (forward displacement of the tip). When the tip comes into contact with the sample surfaces, the conductances show saturation; the saturated values are different depending on the surfaces. The 7×7 surface shows a larger conductance than the Si(100) surface, whereas its value is found to decrease by adsorption of oxygen onto the 7×7 surface, presumably because oxygen saturates the dangling bonds and reduces the density of surface state. These measurements suggest that excess leakage conductance via the point

contact between the STM tip and the clean 7×7 surface is due to current paths parallel to the surface, in other words, the surface-state conductance through the dangling-bond surface state. Its conductance is estimated to be around $10^{-6} \Omega^{-1}$.

Another approach to measuring semiconductor surface conductance with STM relies on fabricating nanoscale structures on the surface using the STM [19]. Heike et al. first fabricated thin insulating trenches on the 7×7 clean surface, by applying a relatively high bias voltage with a high tunnelling current in the STM. After that, they observed the structured surface in a conventional STM mode. Fig. 11(a) and (b) shows a half-closed tape-shaped pattern, surrounded by the insulating trench. The apparent height of the surface area surrounded by the trench is lower (darker) (by approximately 0.2 nm) in the empty-state images (b) as the STM tip approaches to the closed-end of the tape, while the brightness of the whole tape area is observed to be flat in the filled-state images (a).

This result is interpreted as follows: The electrons tunnelling from the tip to the sample flow along the tape through the surface state of only the region restricted by the trench, when the tip is positioned inside the tape (see the top panel in Fig. 11). This is because a Schottky barrier between the surface state and the bulk state forces the current to travel along the surface for a while before leaking into the bulk state. Then, a voltage drop occurs along the tape due to a finite resistance of the surface state, as measured in Fig. 11(c). This is a kind of scanning tunnelling potentiometry [51–53]. By comparing the measured voltage drop along the tape with the calculated one, the conductance of the dangling-bond surface state on the 7×7 surface was deduced to be $8.7 \times 10^{-9} \Omega^{-1}$.

This value is much smaller than that obtained by the point-contact method of Hasegawa(Y) et al. mentioned above. Heike et al. [19] suggest that this discrepancy arises because the method of Hasegawa(Y) et al. involves the conductance through the surface space-charge layer as well as through the surface states. It is postulated that tunnel contact may be a much more effective way to inject carriers into the surface-state bands, whereas direct contact between the probe and sample surface

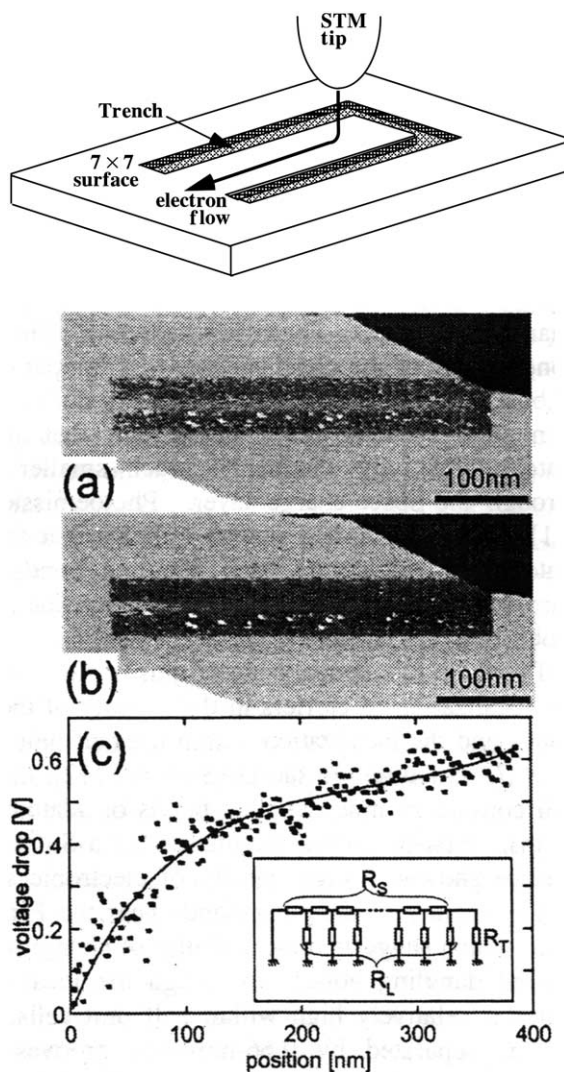


Fig. 11. Top Panel: Schematic diagram of preferred direction of current flow along an artificial nanostructure on a Si(111)- 7×7 clean surface. STM images of (a) the filled-state and (b) empty-state on this surface [19]. In (a), the area surrounded by the trench looks flat, while in (b) the area looks darker with approaching the right end of the area. In (c) the voltage drop measured along the tape-shaped area in (b) is shown, together with a simulation of the voltage drop calculated using a simple series resistance model (calculation is solid line, as modeled in inset).

injects carriers into both of the bulk and surface bands. However, because all ‘one-point’ measurements are susceptible to resistance effects at the point of contact, which are difficult to control or

calculate, multi-probe techniques are essential to resolve these issues.

4.2. Macroscopic four-point probes

Recently, measurements of surface conductivity using four probes with a macroscopic distance were performed in situ on silicon surfaces [13,54]. An example of the sample holder used for such measurements is illustrated in Fig. 12, which is designed for simultaneous metal deposition and reflection high energy diffraction RHEED observations, to prepare well-defined surface superstructures on the whole area of surface [54]. After preparing the superstructures, a small direct current is fed into the specimen crystal through the end clamp electrodes, and the voltage drop is measured between a pair of thin Ta-wire contacts, the spacing of which is usually as large as about 5–10 mm.

Surface-state electrical conduction can be detected in this configuration only under special

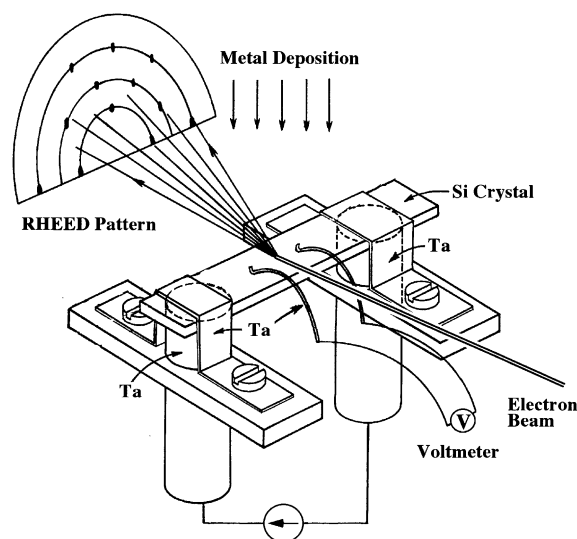


Fig. 12. A sample holder for in-situ electrical conductivity measurements in UHV using a “four-probe” method [54]. The inner probe spacing is typically several millimetres. After the surface superstructures are confirmed by using RHEED, the electron beam is always turned off during the subsequent conductivity measurements. A small current is fed through the clamps at both ends, and the voltage drop is measured by a pair of Ta wire contacts.

conditions, when small amounts (around 0.01 ML) of atoms of monovalent metals (noble and alkali metals) are deposited on top of the Si(111)– $\sqrt{3} \times \sqrt{3}$ -Ag surface. These adatoms are found to enhance the surface conductivity [55]. From photoemission measurements to reveal the changes in surface electronic states, it has been shown that the adatoms donate their valence electrons into the 2D-free-electron-like surface-state band S_1 of the $\sqrt{3} \times \sqrt{3}$ -Ag substrate (Fig. 7(b)), thus enhancing the surface-state conductivity [17,55]. This is quite similar to in bulk crystals of semiconductor in which impurity atoms act as donors or acceptors to vary the carrier concentrations and conductivity.

With increasing the coverage of the adatoms up to around 0.15 ML, 2D islands nucleate and arrange to make a new ordered structure with a $\sqrt{21} \times \sqrt{21}$ periodicity [13,56]. The $\sqrt{21} \times \sqrt{21}$ superstructures made by monovalent-metal-atom adsorptions on the Si(111)– $\sqrt{3} \times \sqrt{3}$ -Ag surface have high surface conductivities. This is due to new dispersive metallic surface-state bands that are created in the superstructures, while the surface-space-charge-layer conductance is suppressed [57,58]. In these cases, the surface-state electrical conduction is so large that it can be detected experimentally using the macroscopic four-probe method. The conductances for these structures are on the order of $10^{-4} \Omega^{-1}$, which is higher than that of the 7×7 clean surface by about four orders of magnitude.

4.3. Microscopic four-point probes

From the expectation of enhanced surface sensitivity by reducing the probe spacings as shown in Fig. 4, micro-four-point probes with probe spacings down to 2 μm have recently been developed using silicon-based micro-fabrication technology [20], one of which is shown in Fig. 13. Such microscopic probes also enable mapping of the local conductivity distribution on material surfaces [59].

The micro-four-point probes have been used in UHV to measure the surface conductances of the Si(111)– 7×7 clean and $\sqrt{3} \times \sqrt{3}$ -Ag surfaces. Fig. 14(a) is a scanning electron micrograph showing a micro-four-point probe of 8 μm spacing, contacting to a silicon surface for the electrical

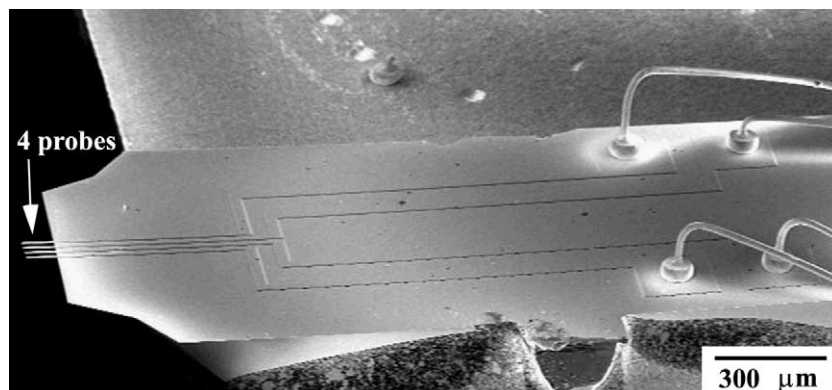


Fig. 13. A SEM image of a silicon chip with a micro-four-point-probe array projecting over the chip edge. The probes are made of silicon oxide, coated with metal. Bonding pads on the chip facilitate electrical connections to the probes. An underetching technique ensures that the probes are not shorted when a metallic layer is evaporated over the whole chip to make the probes conducting. The whole chip is $6 \times 4 \text{ mm}^2$ and mounted on a ceramic holder for convenience [20].

measurements. The resistance measured in this way on the $\sqrt{3} \times \sqrt{3}$ -Ag surface was smaller than that for the 7×7 clean surface by about two orders of magnitudes [22]. This should be compared with the result obtained by macroscopic four probes of about 10 mm probe spacing, where the difference of resistance between the two surfaces was as small as about 10% [60]. These results imply that reducing the probe spacing makes the measurements more surface sensitive, as expected from Fig. 4.

From a quantitative analysis, the extremely high conductance of the $\sqrt{3} \times \sqrt{3}$ -Ag surface compared with that of the 7×7 surface cannot be explained by the surface-space-charge-layer conductivity. Rather it must be attributed to the surface-state band inherent in the $\sqrt{3} \times \sqrt{3}$ -Ag superstructure [20]. Although the surface-state conductivity on this surface had been detected by macroscopic four-probe measurements as a carrier-doping effect into the surface-state band, as mentioned before, micro-four-point probes enabled the direct detection of the contribution of the surface-state conductance [20,22].

Atomic steps on the surface scatter the surface-state electrons as seen as standing waves in Fig. 7(c). This should cause additional electrical resistance at steps, which has been measured with the micro-four-point probe. A technique to control the step configuration on the surface recently has been developed [61], which has been utilized to obtain

almost step-free terraces as wide as the probe spacing, as shown in Fig. 14(b). The surface exhibits flat terraces of about $10 \mu\text{m}$ wide and step bunches of about $2 \mu\text{m}$ wide where around 300 monatomic steps are accumulated. It is wholly covered homogeneously by the 7×7 superstructure or $\sqrt{3} \times \sqrt{3}$ -Ag superstructure due to 1 ML Ag deposition.

By observing the probes and the sample surface by scanning electron microscopy in situ, the probes can be positioned on a large flat terrace, or positioned across a step bunch running between the inner pair of probes. Fig. 14(a) illustrates the latter case. In this way, the surface area under measurement can be selected by shifting the probe position, so that the influence of atomic steps upon the surface conductivity can be intentionally avoided or included. It has been found then that the resistance measured across a step bunch is much larger than that measured on a step-free terrace. Although this result is intuitively reasonable, it is the first direct transport measurement, confirming that atomic steps on a surface causes an additional resistance [22].

4.4. Multi-tip STM

In order to measure the local conductivity in smaller areas down to nanometre scales, several groups have constructed multi-tip STMs in which

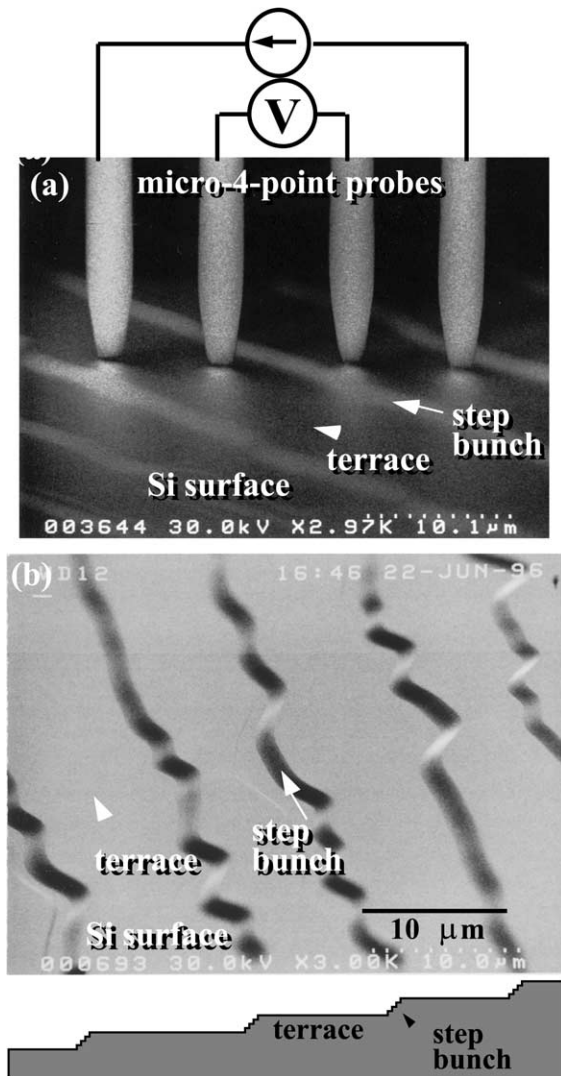


Fig. 14. Panel (a): Scanning electron micrographs showing the micro-four-point probe contacting to a silicon surface for measuring the conductivity in UHV. Slightly brighter bands on the sample surface are step bunches, and wider darker bands are terraces [21]. Panel (b): Grazing-incidence scanning electron micrographs of a Si(111) specimen surface, with step bunching as illustrated at the bottom. The surface is wholly covered by the $\sqrt{3} \times \sqrt{3}$ -Ag surface superstructure with 1 ML Ag.

the tips are utilized as nanoprobe to measure electric properties. The technical challenge of contacting independent probes is considerably greater than using the monolithic micro-four point probe described above. The advantages are that

each probe can be controlled much more accurately with variable probe spacings, and smaller probe spacings could be achievable. Prospects for such multi-tip STMs are the measurement of electrical conductivity in a single domain of a surface superstructure, and the study of ballistic transport as well as other quantum phenomena that occur only on the nanometre scale. The usefulness of double-tip STM has been discussed in Ref. [62].

The first trial to make such an STM was done with electrically isolated two tips mounted on a single scanning head, so that the probe spacing could not be changed [63]. A machine with independently driven double tips in UHV was later constructed by Aono et al. [64], in which the tips can be brought together as close as about 100 nm. The macroscopic radius of each tip determines the minimum distance attainable between the two tips. Such tips can be used as an emitter and collector, like in the point-contact transistor, with much better control on much more well-defined surfaces.

Fig. 15 shows SEM images of four STM tips that are independently driven on a single stage in UHV [23]. With such a device, the surface conductivities were measured as a function of probe spacing ranging from 1 mm to 1 μ m [23]. The results were in accord with the expectation from Fig. 4. The probe-spacing dependences of the measured resistance for the 7×7 clean surface and the $\sqrt{3} \times \sqrt{3}$ -Ag surface were quite different from each other, indicating quite different ways of current flowing; the current flows dominantly only at the surface for the latter superstructure, while the bulk conductivity is dominant for the former superstructure. Such measurements lead to clarifying the influence of surface defects and intrinsic nature of surface-state transport in a more detailed way.

5. Concluding remarks

In the present paper, by taking the silver- and indium-covered Si(111) surfaces as well as the clean surface as examples, various phenomena revealed in the surface-state bands and electronic transport phenomena are described. Some of the readers may think that it is neither surprising nor

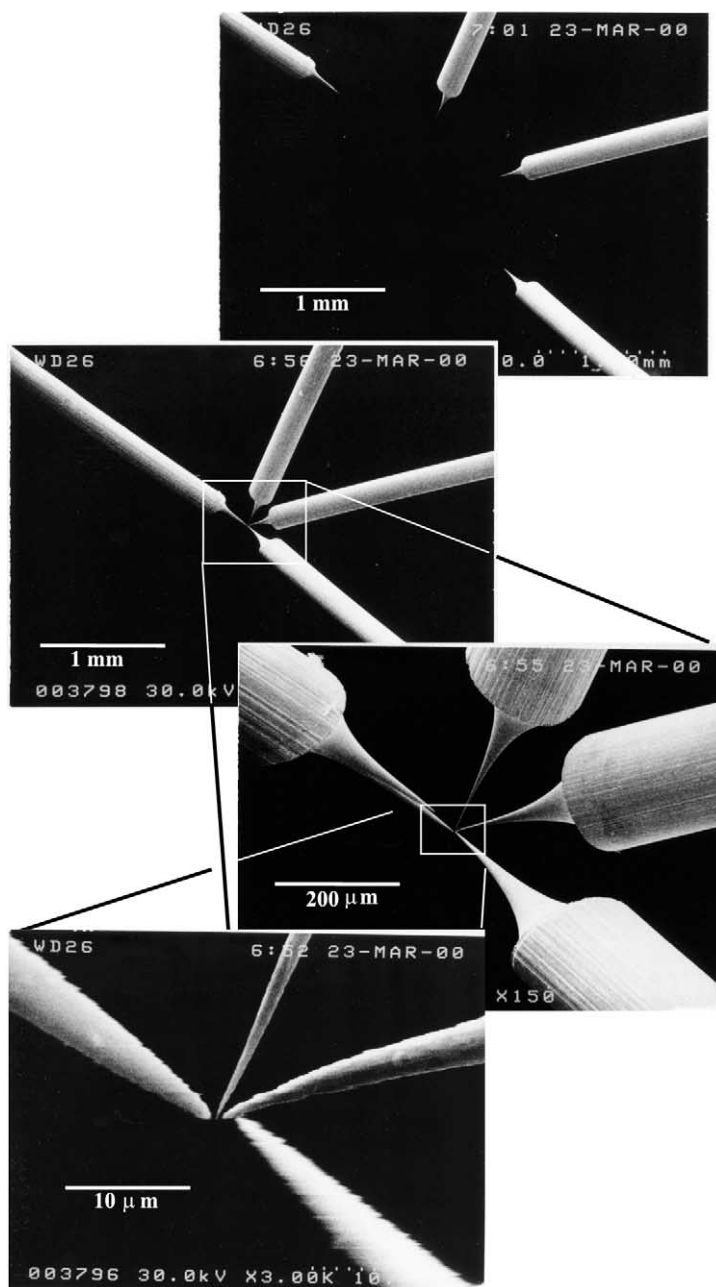


Fig. 15. SEM images of four STM tips, independently driven in UHV [23]. The tips are separated as far as about 1 mm in the top panel, while they are brought together to within a distance less than 1 μm spacing in the other panels.

new to have metallic electronic states and enhanced conductivity on these surfaces because ‘metal’ atoms are deposited on the surface. But such considerations are too naive. The deposited

metal atoms do not exhibit their own properties expected from their bulk crystals. The metal atoms do not make metallic bonds with each other to produce conduction electrons like in their bulks,

rather make bonds with the substrate Si atoms to form characteristic surface electronic states. This is the main point for the properties of surface phases as new ‘nanomaterials’, which are completely different from those of bulk materials of composite atoms. The atomic arrangements on the surface and the resulting electronic states directly characterize the transport properties.

The electronic transport properties of surface-state bands are increasingly important subjects in the near future because of necessity for semiconductor devices as well as interest in fundamental physics. With progress in miniaturization of microelectronics devices, the signal currents are forced to flow only near the surface region of semiconductor crystals. Eventually the signals are expected to process with current flow only through one or two atomic layers, where the surface electronic states play main roles instead of the bulk states. Therefore the studies of transport properties of surfaces lead to an important branch of nanotechnology when coupled with the fabrication technology for atomic-scale structures on surfaces. For that, the microscopic multi-probes described here are indispensably important. Thus it is tempting to conclude that the descendants of the point-contact transistor are still having a major impact on surface science—and microelectronics—more than half a century later.

Acknowledgements

Dr. Tadaaki Nagao and other members of the group in University of Tokyo are acknowledged for their supportive collaboration. Dr. Ichiro Shiraki of University of Tokyo and Drs. Christian L. Petersen, Peter Bøggild, Torben M. Hansen at MIC (Technical University of Denmark) are acknowledged for their dedicated contributions to micro-four-point probe measurements. Professor Martin Henzler at Hannover University gave us valuable advice on surface-state conduction. The preparation of this manuscript, as well as some of the work described here was supported in part by Grants-in-Aid from the Ministry of Education, Science, Culture, and Sports of Japan, especially through that for Creative Basic Research (no.

09NP1201) conducted by Professor Katsumichi Yagi of Tokyo Institute of Technology, and also for International Collaboration Program (no. 11694059). One of us (S.H.) has also been supported also by Core Research for Evolutional Science and Technology of the Japan Science and Technology Corporation conducted by Professor Masakazu Aono of Osaka University and RIKEN.

References

- [1] W. Shockley, G.L. Pearson, Modulation of conductance of thin films of semiconductors by surface charges, *Phys. Rev.* 74 (1948) 232.
- [2] J. Bardeen, Surface states and rectification at a metal–semiconductor contact, *Phys. Rev.* 71 (1947) 717.
- [3] J. Bardeen, W.H. Brattain, The transistor a semiconductor triode, *Phys. Rev.* 74 (1948) 230; For a popular introduction to this discovery, see M. Riordan, L. Hoddeson, *Crystal Fire*, Norton Publishers, 1997.
- [4] W. Shockley, The theory of p–n junctions in semiconductors and p–n junction transistors, *Bell Sys. Tech. J.* 28 (1949) 435.
- [5] V.G. Lifshits, A.A. Saranin, A.V. Zotov, *Surface Phases on Silicon*, Wiley, Chichester, 1994.
- [6] For example H. Lüth, *Surfaces and Interfaces of Solids*, Springer, Berlin, 1993.
- [7] G. Binnig, H. Rohrer, Scanning tunnelling microscopy—from birth to adolescence, *Rev. Mod. Phys.* 59 (1987) 615.
- [8] M.F. Crommie, C.P. Lutz, D.M. Eigler, E.L. Heller, Waves on a metal surface and quantum corrals, *Surf. Rev. Lett.* 2 (1995) 127.
- [9] Ph. Avouris, I.-W. Lyo, R.E. Walkup, Y. Hasegawa, Real space imaging of electron scattering phenomena at metal surfaces, *J. Vac. Sci. Technol. B* 12 (1994) 1447.
- [10] K. Takayanagi, Y. Tanishiro, S. Takahashi, M. Takahashi, Structure analysis of Si(111)- 7×7 reconstructed surface by transmission electron diffraction, *Surf. Sci.* 164 (1985) 367.
- [11] For example S. Datta, *Electronic Transport in Mesoscopic Systems*, Cambridge, New York, 1995.
- [12] M. Henzler, Electronic transport at surfaces, in: J.M. Blakely (Ed.), *Surface Physics of Materials I*, Academic Press, New York, 1975, p. 241.
- [13] For review S. Hasegawa, X. Tong, S. Takeda, N. Sato, T. Nagao, Structures and electronic transport on silicon surfaces, *Prog. Surf. Sci.* 60 (1999) 89; S. Hasegawa, Surface-state bands on silicon as electron systems in reduced dimensions at atomic scales, *J. Phys. C: Condens. Matter* 12 (2000) R463.
- [14] W.H. Brattain, J. Bardeen, Surface properties of germanium, *Bell Syst. Tech. J.* 32 (1953) 1.

- [15] J. Bardeen, S.R. Morrison, Surface barriers and surface conductance, *Physica* 20 (1954) 873.
- [16] W. Mönch, On the correlation of geometrical structure and electronic properties at clean semiconductor surfaces, *Surf. Sci.* 63 (1977) 79.
- [17] Y. Nakajima, S. Takeda, T. Nagao, S. Hasegawa, X. Tong, Surface electrical conduction due to carrier doping into a surface-state band on Si(111)- $\sqrt{3} \times \sqrt{3}$ -Ag, *Phys. Rev. B* 56 (1997) 6782.
- [18] S. Hasegawa, Atomic imaging of macroscopic surface conductivity, *Curr Opin Solid State Mater. Sci.* 4 (1999) 429.
- [19] S. Heike, S. Watanabe, Y. Wada, T. Hashizume, Electron conduction through surface states of the Si(111)-(7 × 7) surface, *Phys. Rev. Lett.* 81 (1998) 890.
- [20] C.L. Petersen, F. Grey, I. Shiraki, S. Hasegawa, Microfour-point probe for studying electronic transport through surface states, *Appl. Phys. Lett.* 77 (2000) 3782. Microfour-point probes are now commercially available; <http://www.capres.com>.
- [21] I. Shiraki, C.L. Petersen, P. Bøggild, T.M. Hansen, T. Nagao, F. Grey, S. Hasegawa, Microfour-point probes in a UHV-scanning electron microscope for in-situ surface conductivity measurements, *Surf. Rev. Lett.* 7 (2000) 533.
- [22] I. Shiraki, C.L. Petersen, P. Bøggild, T.M. Hansen, T. Nagao, F. Grey, S. Hasegawa, Surface electronic transport measured with microfour-point probes, *Nature*, submitted for publication.
- [23] I. Shiraki, F. Tanabe, R. Hobarra, T. Nagao, S. Hasegawa, Independently driven four-tip probes for conductivity measurements in ultrahigh vacuum, *Surf. Sci.*, 493 (2001) 633.
- [24] D.M. Eigler, E.K. Schweizer, Positioning single atoms with a scanning tunnelling microscope, *Nature* 344 (1990) 524–526; J.A. Stroscio, D.M. Eigler, Atomic and molecular manipulation with the scanning tunnelling microscope, *Science* 254 (1991) 1319.
- [25] F.J. Himpsel, G. Hollinger, R.A. Pollak, Determination of the Fermi-level pinning position at Si(111) surfaces, *Phys. Rev. B* 28 (1983) 7014.
- [26] J. Viernow, M. Henzler, W.L. O'Brien, F.K. Men, F.M. Leibsle, D.Y. Petrovykh, J.L. Lin, F.J. Himpsel, Unoccupied surface states on Si(111) $\sqrt{3} \times \sqrt{3}$ -Ag, *Phys. Rev. B* 57 (1998) 2321.
- [27] T. Takahashi, S. Nakatani, N. Okamoto, T. Ishikawa, S. Kikuta, Study on the Si(111) $\sqrt{3} \times \sqrt{3}$ -Ag surface structure by X-ray diffraction, *Jpn. J. Appl. Phys.* 27 (1988) L753; T. Takahashi, S. Nakatani, N. Okamoto, T. Ishikawa, S. Kikuta, A study of the Si(111) $\sqrt{3} \times \sqrt{3}$ -Ag surface by transmission X-ray diffraction and X-ray diffraction topography, *Surf. Sci.* 242 (1991) 54; T. Takahashi, S. Nakatani, Refinement of the Si(111) $\sqrt{3} \times \sqrt{3}$ -Ag structure by surface X-ray diffraction, *Surf. Sci.* 282 (1993) 17, and references therein.
- [28] M. Katayama, R.S. Williams, M. Kato, E. Nomura, M. Aono, Structure analysis of the Si(111) $\sqrt{3} \times \sqrt{3}$ R30°-Ag surface, *Phys. Rev. Lett.* 66 (1991) 2762.
- [29] E. Vlieg, E. Fontes, J.R. Patel, Structure analysis of Si(111)-($\sqrt{3} \times \sqrt{3}$)R30°/Ag using X-ray standing waves, *Phys. Rev. B* 43 (1991) 7185.
- [30] L.S.O. Johansson, E. Landemark, C.J. Karlsson, R.I.G. Uhrberg, Fermi-level pinning and surface-state band structure of the Si(111)/($\sqrt{3} \times \sqrt{3}$)R30°Ag surface, *Phys. Rev. Lett.* 63 (1989) 2092; L.S.O. Johansson, E. Landemark, C.J. Karlsson, R.I.G. Uhrberg, Structure of the ($\sqrt{3} \times \sqrt{3}$)R30° Ag/Si(111) surface from first-principles calculations, *Phys. Rev. Lett.* 69 (1992) 2451.
- [31] S. Hasegawa, N. Sato, I. Shiraki, C.L. Petersen, P. Bøggild, T.M. Hansen, T. Nagao, F. Grey, Surface-state bands on silicon—Si(111)- $\sqrt{3} \times \sqrt{3}$ -Ag surface superstructure, *Jpn. J. Appl. Phys.* 39 (2000) 3815.
- [32] N. Sato, S. Takeda, T. Nagao, S. Hasegawa, Electron standing waves on the Si(111)- $\sqrt{3} \times \sqrt{3}$ -Ag surface, *Phys. Rev. B* 59 (1999) 2035.
- [33] T. Yokoyama, M. Okamoto, K. Takayanagi, Electron waves in the π^* -surface band of the Si(001) surface, *Phys. Rev. Lett.* 81 (1998) 3423; T. Yokoyama, K. Takayanagi, Size quantization of surface-state electrons on the Si(001) surface, *Phys. Rev. B* 59 (1999) 12232.
- [34] L. Li, W.-D. Schneider, R. Berndt, S. Crampin, Electron confinement to nanoscale Ag islands on Ag(111): a quantitative study, *Phys. Rev. Lett.* 80 (1998) 3332.
- [35] D. Fujita, K. Amemiya, T. Yakabe, H. Nejoh, Anisotropic standing-wave formation on an Au(111)-(23 × $\sqrt{3}$) reconstructed surface, *Phys. Rev. Lett.* 78 (1997) 3904.
- [36] L. Petersen, P.T. Sprunger, Ph. Hofmann, E. Lægsgaard, B.G. Briner, M. Doering, H.-P. Rust, A.M. Bradshaw, F. Besenbacher, E.W. Plummer, Direct imaging of the two-dimensional Fermi contour: Fourier-transform STM, *Phys. Rev. B* 57 (1998) R6858.
- [37] R. Losio, K.N. Altmann, F.J. Himpsel, Fermi surface of Si(111)7 × 7, *Phys. Rev. B* 61 (2000) 10845.
- [38] F. Flores, A. Levy Yeyati, J. Ortega, Metal–insulator transition in the Si(111)-(7 × 7) surface, *Surf. Rev. Lett.* 4 (1997) 281.
- [39] A.A. Saranin, V.G. Lifshits, M. Katayama, K. Oura, Composition and surface structure of quantum chains on a In/Si(111) surface, *Jpn. J. Appl. Phys.* 39 (2000) L306.
- [40] O. Bunk, G. Falkenberg, J.H. Zeysing, L. Lottermoser, R.L. Johnson, M. Nielsen, F. Berg-Rasmussen, J. Baker, R. Feidenhans'l, Structure determination of the indium-induced Si(111)-(4 × 1) reconstruction by surface X-ray diffraction, *Phys. Rev. B* 59 (1999) 12228.
- [41] J. Nakamura, S. Watanabe, M. Aono, Anisotropic electronic structure of the Si(111)-(4 × 1)-In surface, *Phys. Rev. B* 63 (2001) 193307.
- [42] T. Abukawa, M. Sasaki, F. Hisamatsu, T. Goto, T. Kinoshita, A. Kakizaki, S. Kono, Surface electronic structure of a single-domain Si(111)4 × 1-In surface: a

- synchrotron radiation photoemission study, *Surf. Sci.* 325 (1995) 33.
- [43] I.G. Hill, A.B. McLean, Metallicity of In chains on Si(111), *Phys. Rev. B* 56 (1997) 15725.
- [44] R.E. Peierls, *Quantum Theory of Solids*, Clarendon Press, Oxford, 1964.
- [45] H.W. Yeom, S. Takeda, E. Rotenberg, I. Matsuda, K. Horikoshi, J. Schaefer, C.M. Lee, S.D. Kevan, T. Ohta, T. Nagao, S. Hasegawa, Instability and charge density wave of metallic quantum chains on a silicon surface, *Phys. Rev. Lett.* 82 (1999) 4898.
- [46] O. Gallus, Th. Pillo, M. Hengsberger, P. Segovia, Y. Baer, A system with a complex phase transition: Indium chains on Si(111), *Eur. Phys. J. B* 20 (2001) 313.
- [47] C. Kumpf, O. Bunk, J.H. Zeysing, Y. Su, M. Nielsen, R.L. Johnson, R. Feidenhans'l, K. Bechgaard, Low-temperature structure of indium quantum chains on silicon, *Phys. Rev. Lett.* 85 (2000) 4916.
- [48] T. Nishiguchi, M. Kageshima, N. Ara-Kato, A. Kawazu, Behavior of charge density waves in a one-dimensional organic conductor visualized by scanning tunneling microscopy, *Phys. Rev. Lett.* 81 (1998) 3187.
- [49] M. Ishida, T. Mori, H. Shigekawa, Surface charge-density wave on the one-dimensional organic conductor β -(BEDT-TTF) $_2$ PF $_6$, *Phys. Rev. Lett.* 83 (1999) 596.
- [50] Y. Hasegawa, I.-W. Lyo, Ph. Avouris, Measurement of surface state conductance using STM point contacts, *Surf. Sci.* 357/358 (1996) 32.
- [51] J.R. Kirtley, S. Washburn, M.J. Brady, Direct measurement of potential steps at grain boundaries in the presence of current flow, *Phys. Rev. Lett.* 60 (1988) 1546.
- [52] A.D. Kent, I. Maggio-Aprile, Ph. Niedermann, O. Fischer, Direct measurements of the effects of inhomogeneities on the normal-state transport properties of YBaCuO thin films, *Phys. Rev. B* 39 (1989) 12363.
- [53] P. Muralt, GaAs pn junction studied by scanning tunneling potentiometry, *Appl. Phys. Lett.* 49 (1986) 1441; P. Muralt, H. Meier, D.W. Pohl, H.W.M. Salemink, Scanning tunneling microscopy and potentiometry on a semiconductor heterojunction, *Appl. Phys. Lett.* 50 (1987) 1352.
- [54] S. Hasegawa, S. Ino, Surface structures and conductance at epitaxial growths of Ag and Au on the Si(111) surface, *Phys. Rev. Lett.* 68 (1992) 1192.
- [55] Y. Nakajima, G. Uchida, T. Nagao, S. Hasegawa, Two-dimensional adatom gas on the Si(111)- $\sqrt{3} \times \sqrt{3}$ -Ag surface detected through changes in electrical conduction, *Phys. Rev. B* 54 (1996) 14134.
- [56] S. Hasegawa, K. Tsuchie, K. Toriyama, X. Tong, T. Nagao, Surface electronic transport on silicon: donor- and acceptor-type adsorbates on Si(111)- $\sqrt{3} \times \sqrt{3}$ -Ag substrate, *Appl. Surf. Sci.* 162/163 (2000) 42.
- [57] X. Tong, C.-S. Jiang, S. Hasegawa, Electronic structure of the Si(111)- $\sqrt{21} \times \sqrt{21}$ -(Ag + Au) surface, *Phys. Rev. B* 57 (1998) 9015.
- [58] X. Tong, C.-S. Jiang, K. Horikoshi, S. Hasegawa, Surface-state electrical conduction on the Si(111)- $\sqrt{3} \times \sqrt{3}$ -Ag surface with noble-metal adatoms, *Surf. Sci.* 449 (2000) 125.
- [59] P. Böggild, T.M. Hanssen, O. Kuhn, F. Grey, T. Junno, L. Montelius, Scanning nanoscale multiprobes for conductivity measurements, *Rev. Sci. Instrum.* 71 (2000) 2781–2783; P. Böggild, F. Grey, T. Hanssenkam, D.R. Greve, T. Bjornholm, Direct measurement of the microscale conductivity of conjugated polymer monolayers, *Adv. Mater.* 12 (2000) 947.
- [60] C.-S. Jiang, S. Hasegawa, S. Ino, Surface conductivity for Au or Ag on Si(111), *Phys. Rev. B* 54 (1996) 10389.
- [61] T. Ogino, Self-organization of nanostructures on Si wafers using surface structure control, *Surf. Sci.* 386 (1997) 137.
- [62] Q. Niu, M.C. Chang, C.K. Shih, Double-tip scanning tunneling microscope for surface analysis, *Phys. Rev. B* 51 (1995) 5502.
- [63] S. Tsukamoto, B. Siu, N. Nakagiri, Twin-probe scanning tunneling microscope, *Rev. Sci. Instrum.* 62 (1991) 1767.
- [64] M. Aono, C.-S. Jiang, T. Nakayama, T. Okuda, S. Qiao, M. Sakurai, C. Thirstrup, Z.-H. Wu, The present and future of nano-lithography using scanning probes—how to measure the properties of nano-lithographed surfaces, *J. Surf. Sci. Soc. Jpn.* 9 (1998) 698, in Japanese.